AIP | Applied Physics Letters

# Enhanced tunneling magnetoresistance and perpendicular magnetic anisotropy in Mo/CoFeB/MgO magnetic tunnel junctions

H. Almasi, D. Reifsnyder Hickey, T. Newhouse-Illige, M. Xu, M. R. Rosales, S. Nahar, J. T. Held, K. A. Mkhoyan, and W. G. Wang

Citation: Applied Physics Letters **106**, 182406 (2015); doi: 10.1063/1.4919873
View online: http://dx.doi.org/10.1063/1.4919873
View Table of Contents: http://scitation.aip.org/content/aip/journal/apl/106/18?ver=pdfcov
Published by the AIP Publishing



# Enhanced tunneling magnetoresistance and perpendicular magnetic anisotropy in Mo/CoFeB/MgO magnetic tunnel junctions

H. Almasi,[1] D. Reifsnyder Hickey,[2] T. Newhouse-Illige,[1] M. Xu,[1] M. R. Rosales,[1] S. Nahar,[3] J. T. Held,[2] K. A. Mkhoyan,[2] and W. G. Wang[1,a)]
[1]*Department of Physics, University of Arizona, Tucson, Arizona 85721, USA*
[2]*Department of Chemical Engineering and Materials Science, University of Minnesota, Minneapolis, Minnesota 55455, USA*
[3]*Science Department, Sunnyside High School, Tucson, Arizona 85706, USA*

(Received 13 February 2015; accepted 1 April 2015; published online 6 May 2015)

Structural, magnetic, and transport studies have been performed on perpendicular magnetic tunnel junctions (pMTJ) with Mo as the buffer and capping layers. After annealing samples at 300 °C and higher, consistently better performance was obtained compared to that of conventional pMTJs with Ta layers. Large tunneling magnetoresistance (TMR) and perpendicular magnetic anisotropy (PMA) values were retained in a wide range of samples with Mo layers after annealing for 2 h at 400 °C, in sharp contrast to the junctions with Ta layers, in which superparamagnetic behavior with nearly vanishing magnetoresistance was observed. As a result of the greatly improved thermal stability, TMR as high as 162% was obtained in junctions containing Mo layers. These results highlight the importance of the heavy-metal layers adjacent to CoFeB electrodes for achieving larger TMR, stronger PMA, and higher thermal stability in pMTJs. © *2015 AIP Publishing LLC*.
[http://dx.doi.org/10.1063/1.4919873]

Magnetic tunnel junction (MTJ) is one of the most important structures in spintronic research.[1–6] In particular, perpendicularly magnetized magnetic tunnel junction (pMTJ) is a promising candidate for next-generation ultra-low energy memory and logic devices due to its long retention, small footprint, fast switching, and high endurance.[7–14] In general, three types of pMTJs have been investigated. The first one utilizes the strong bulk perpendicular magnetic anisotropy (PMA) of thin films based on rare-earth[7] or $L1_0$ magnetic alloys.[8] The second type uses a Co/Pt (Pd) superlattice exchange-coupled to CoFeB,[9,10] in which the CoFeB layer provides a large spin polarization and the superlattice beneath provides strong PMA. The third type employs interfacial PMA in heavy-metal/ferromagnet/oxide (HM/FM/oxide) structures,[11,12,15] which can produce high tunneling magnetoresistance (TMR) with fewer materials compared to structures with superlattices. In addition to TMR and PMA, interesting phenomena, such as spin-orbit switching[16] and voltage-controlled magnetism,[17,18] have also been studied in HM/FM/oxide structures.

For many applications, a pMTJ with large TMR, strong PMA, and robust thermal stability is highly desired.[13,14] The interfacial magnetic anisotropy energy is generally 1–2 erg/cm$^2$ in HM/FM/oxide structures.[11,19,20] Previous studies on these pMTJs have shown a rapid decrease in the TMR during post-growth thermal annealing, which was attributed to the loss of antiparallel (AP) states due to decreased PMA at high temperatures.[21,22] In most MTJ studies, the HM layer has been tantalum, owing to its amorphous nature at small thicknesses and its reasonably good thermal stability. It was demonstrated that the interfacial PMA in Ta/CoFeB/MgO heterostructures can be increased by up to 20% when the Ta buffer layer is doped with nitrogen.[23] It also has been shown that when hafnium[24] or molybdenum[20] was used as the buffer layer instead of Ta, a substantially larger PMA and greatly enhanced thermal stability during annealing can be achieved. However, no report exists on the transport properties of MTJs with these HM layers.

In this work, we studied the structural, magnetic, and transport properties of pMTJs with Mo as the buffer and capping layers. Compared to conventional pMTJs with Ta, a larger TMR was consistently observed across samples with various MgO thicknesses and over an annealing-temperature range of 300–400 °C. Although the perpendicular easy axis in all MTJs with Ta layers was entirely lost after thermal annealing for 2 h at 400 °C, reasonably strong PMA up to 0.3 erg/cm$^2$ was maintained in Mo-based MTJs with CoFeB layers ranging from 0.7 to 1.2 nm. As a result of the enhanced PMA, a large TMR of 162% was achieved in this study.

All of the samples in this work were deposited onto silicon wafers with 1 $\mu$m of thermal oxide in a 12-source magnetron sputtering system (AJA-International). The deposition system is equipped with a residual gas analyzer for monitoring $H_2O$ partial pressure and the base pressure is in the range of $10^{-9}$ Torr. The substrates were held at ambient temperature during deposition. The metallic layers were deposited by DC magnetron sputtering under an Ar pressure of 2 mTorr. The MgO layer was deposited by RF magnetron sputtering at 1.3 mTorr of Ar. For structural and transport studies, multilayers consisting of Mo(6)/Ru(10)/Mo(10)/$Co_{20}Fe_{60}B_{20}$(0.8)/MgO(1–3)/$Co_{20}Fe_{60}B_{20}$(1.6)/Mo(10)/Ru(20) and Ta(6)/Ru(10)/Ta(10)/$Co_{20}Fe_{60}B_{20}$(0.8)/MgO(1–3)/$Co_{20}Fe_{60}B_{20}$(1.6)/Ta(10)/Ru(20) were used, where the numbers in parentheses indicate the thickness in nanometers. The samples were annealed in a rapid thermal annealing setup in an inert atmosphere. The microstructure was imaged using scanning transmission electron microscopy (STEM), and the

a)Email: wgwang@physics.arizona.edu

 

elemental composition was mapped by energy-dispersive X-ray spectroscopy (EDX). An aberration-corrected (CEOS DCOR probe corrector) FEI Titan G2 60–300S/TEM equipped with a Schottky X-FEG gun and a Super-X quad-SDD windowless in-polepiece EDX detector was used at 200 kV with a probe convergence angle of 16 mrad. For testing TMR, the continuous films were patterned into circular MTJs with diameters of 25 $\mu$m using conventional microfabrication techniques. The magnetic properties of the films were characterized by a vibrating sample magnetometer (VSM, Mirosenese EZ-9). Multilayers consisting of Ta(6)/Ru(10)/Ta(10)/$Co_{20}Fe_{60}B_{20}$(t)/MgO(1-3)/Ta(6) and Mo(6)/Ru(10)/Mo(10)/$Co_{20}Fe_{60}B_{20}$(t)/MgO(1-3)/Ta(6) with $Co_{20}Fe_{60}B_{20}$ thicknesses (t) ranging from 0.6 to 1.7 nm were fabricated for VSM study. All measurements were performed at room temperature.

For many applications, pMTJs are required to be annealed at 400 °C or above.[13,14] The structure integrity of the very thin bottom CoFeB electrode (0.8 nm) is of particular concern at such high temperature. First, we have carried out STEM study to probe the structure and chemical composition of the pMTJ. Figure 1 shows a high-angle annular dark-field STEM (HAADF-STEM) image with the corresponding composite and individual elemental maps for a pMTJ with Mo layer, annealed for 2 h at 400 °C. EDX maps directly reveal the distributions of Mo and Fe (Co), which are hard to obtain from conventional TEM or even HAADF-STEM images due to the close atomic numbers.[25] As can be seen from Figure 1, the integrity of the CoFeB layers as well as the MgO barrier is well maintained after 2 h of annealing at 400 °C.

Next, we studied the TMR of patterned pMTJs under different annealing conditions. For samples annealed at 300 °C for 10 min, both the Ta/CoFeB/MgO and Mo/CoFeB/MgO tunnel junctions show reasonably high TMR >100%, as shown in Figure 2(a). The MTJ with Mo exhibits stronger PMA, as evidenced by the large switching field of the soft layer. The striking difference of these two types of MTJs was revealed after thermal annealing at 400 °C for 2 h, as shown in Figure 2(b). The TMR for the MTJ with Ta as the buffer layer dramatically declined to a value of 4.5% (blue line). Moreover, the TMR curve lost its sharp transition between the AP and P states, suggesting that the PMA is entirely vanished and the CoFeB layer now behaves superparamagnetically. This is in good agreement with previous studies on Ta/CoFeB/MgO MTJs,[21,22] in which annealing at temperatures higher than 350 °C rapidly destroys the PMA and TMR of the structure. In contrast, the MTJ with Mo as the buffer layer showed a more than 20% increase in its TMR values (black line). Despite the smaller coercivity of both the soft and hard layers, sharp magnetic switching with a good AP plateau is clearly seen in the TMR curve. This behavior is consistently observed in all MTJs with MgO thicknesses ranging from 1.8 to 2.5 nm. As shown in Figure 2(c), the TMR is approximately 100%–120% for both types of MTJ after annealing at 300 °C for 10 min. Whereas, the TMR of MTJs with Ta dropped to nearly zero after 2 h of annealing at 400 °C, the TMR of MTJs with Mo increased by approximately 15%–20%. These results clearly demonstrate the superior properties of Mo over the widely used Ta in promoting high TMR after high-temperature annealing, which is a critical feature in many applications of pMTJs.[13,14]

To gain more insight into the behavior of the MTJs with Mo, we compared the TMR and corresponding parallel resistance ($R_p$) after annealing under different conditions. It has been well established that high-temperature post-growth thermal annealing is one of the most essential steps to achieve large TMR in CoFeB/MgO/CoFeB junctions.[26,27] The symmetry-conserved tunneling is only achieved by the

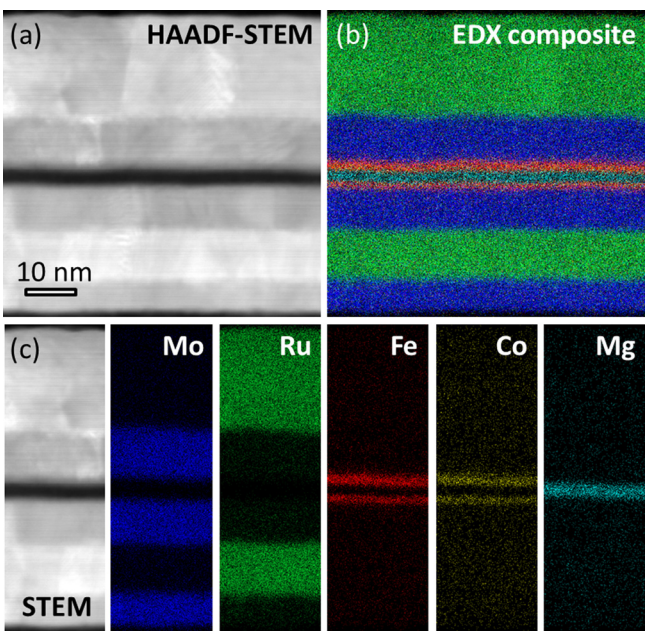


FIG. 1. (a) HAADF-STEM image of the cross section (silicon wafer substrate at bottom) of a Mo-based pMTJ annealed at 400 °C for 2 h. (b) A composite EDX map of the pMTJ composition, for which the assignment of the colors is provided in (c), which shows individual-element slices of a selected region of the composite map in (b), as well as the HAADF slice to which they correspond.

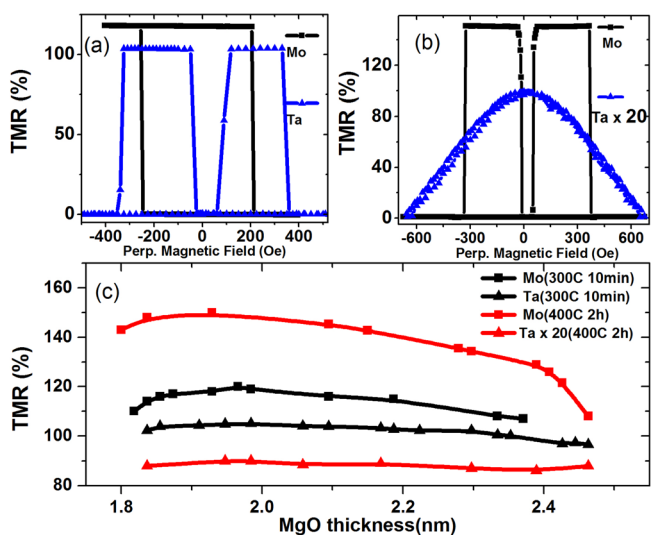


FIG. 2. (a) Normalized TMR curves for Ta/CoFeB/MgO (blue) and Mo/CoFeB/MgO (black) tunnel junctions after annealing at 300 °C for 10 min and (b) after annealing at 400 °C for 2 h. (c) TMR vs. MgO thickness of the MTJs after annealing at 300 °C for 10 min (black lines) and after annealing at 400 °C for 2 h (red lines).

crystallization of amorphous CoFeB electrodes with the templating effect of a (100)-oriented MgO barrier using the solid state epitaxy (SSE) process.[27] The evolution of TMR is dictated by the interplay of the crystallization of CoFeB, improvement in the crystallinity of the MgO, diffusion of impurities into MgO,[26] and modification of the magnetic anisotropy of CoFeB.[21] The TMR for MTJs with various MgO thicknesses for four different annealing conditions is plotted in Figure 3(a). After 10 min of annealing at 300, 350, and 400 °C, the TMR of the junctions steadily increased from approximately 120% to 140%, and then to 160%. The highest TMR of 162% was achieved in the MTJ with an MgO thickness of 1.95 nm (inset of Figure 3(b)). Annealing for 2 h at 400 °C decreased the overall TMR to a level similar to that observed for MTJs after 10 min of annealing at 350 °C. Yet, most of the MTJs retained a large TMR between 120% and 140%.

The corresponding behavior of the $R_p$ of the MTJs is plotted in Figure 3(b). Initially, $R_p$ shows small, steady increases with a short annealing time of 10 min from 300 to 400 °C, followed by a substantial jump (note that the resistance is plotted on a logarithmic scale) after 2 h of annealing at 400 °C. According to the coherent-tunneling theory of MgO-based tunnel junctions, the conductance in the parallel channel is mainly dominated by electrons with $\Delta_1$ symmetry.[5] During thermal annealing, $R_p$ usually experiences a sharp drop in the initial stage due to the buildup of the $\Delta_1$ channel related to the crystallization of CoFeB, followed by a slow increase related to impurities diffusing into the MgO.[26] Simultaneously, the antiparallel resistance ($R_{ap}$) of the MTJ will increase due to the elimination of the $\Delta_5$ and $\Delta_2$ channels. As long as there is no major destruction of the $\Delta_1$ channel, the TMR of the junction will continue increasing if the rate of rise for $R_{ap}$ is larger than that of $R_p$.[26] For the samples that experienced short annealing times, the increase in $R_p$ from 300 to 350 °C and then from 350 to 400 °C is less than the increase in their corresponding antiparallel resistances; therefore, the TMR continues increasing, as shown in Figure 3(a). The reduced TMR for samples annealed at 400 °C for 2 h can be explained from Figure 3(b) by the sharply increased $R_p$ (red line), suggesting that the added impurity scattering of the $\Delta_1$-band electrons due to interdiffusion contributes to this TMR deterioration.[26]

To further confirm the change in the magnetic anisotropy in our samples, we performed VSM measurements on a series of Ta/Ru/Ta/CoFeB/MgO/Ta and Mo/Ru/Mo/CoFeB/MgO/Ta films with various CoFeB thicknesses. These samples were annealed for 2 h at 400 °C. The M-H curves under the out-of-plane and in-plane magnetic fields are shown in Figures 4(a) and 4(b), respectively. The CoFeB thickness in these samples was kept at 0.85 nm, which is the same as in the patterned MTJs. The Mo/CoFeB/MgO sample shows easy-axis-like sharp switching under the out-of-plane field and hard-axis-like switching under the in-plane field. The saturation magnetization (without considering the magnetic dead layer) and anisotropy field are 1150 emu/cm$^3$ and 0.34 erg/cm$^3$, respectively. The Ta/CoFeB/MgO film, on the other hand, shows superparamagnetic behavior for magnetic fields under both orientations, which is in good agreement with the TMR curve shown in Figure 2(b) and in a previous report.[20]

The effective magnetic anisotropy energy in the form of $K_{eff}{\cdot}t_{CoFeB}$ is presented in Fig. 4(c) as a function of the CoFeB thickness. The negative values of $K_{eff}{\cdot}t_{CoFeB}$ correspond to the in-plane anisotropy of the samples. After 2 h of annealing at 400 °C, no Ta/CoFeB/MgO films with perpendicular magnetic anisotropy can be identified in the

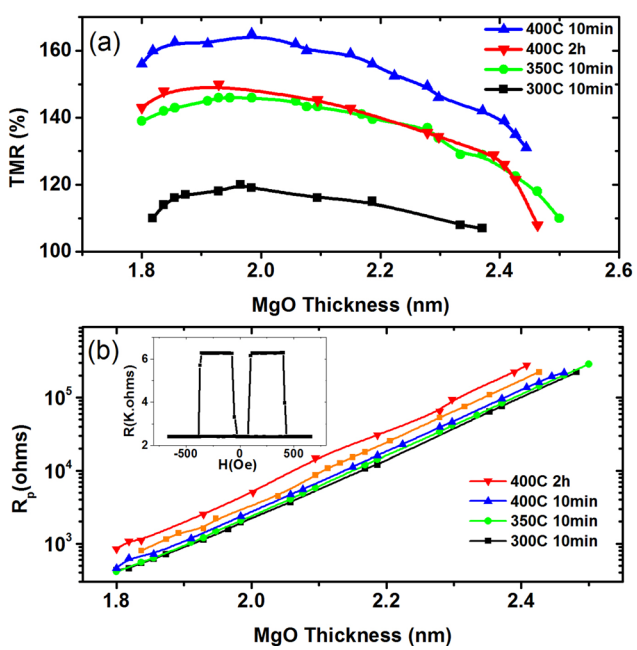


FIG. 3. (a) TMR for Mo/CeFeB/MgO tunnel junctions annealed at 300 °C (black), 350 °C (green), and 400 °C (blue) for 10 min and 400 °C for 2 h (red). (b) Corresponding resistance in the parallel state at various annealing conditions. Inset shows the highest TMR of 162% achieved in this study.

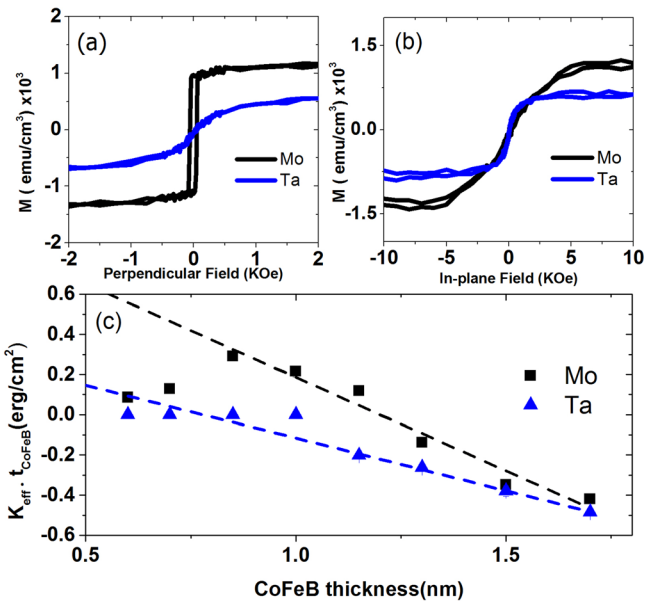


FIG. 4. (a) M-H curves for the Ta/CoFeB (0.85 nm)/MgO and Mo/CoFeB (0.85 nm)/MgO films under the out-of-plane magnetic field. The samples have been annealed at 400 °C for 2 h. (b) Corresponding M-H curves under the in-plane magnetic field. (c) CoFeB thickness dependence of $K_{eff}{\cdot}t_{CoFeB}$ for the two types of samples. Dashed lines are linear fits of the data to determine $K_s$.

whole range of CoFeB thickness, whereas Mo/CoFeB/MgO films show PMA for CoFeB thicknesses of 0.6–1.15 nm. The interfacial magnetic anisotropy ($K_s$) was estimated by a linear fit to the appropriate set of data points, as indicated by the dashed lines. A $K_s$ value of 0.41 erg/cm$^2$ was obtained for Ta/CoFeB/MgO using samples showing a well-defined easy axis. In contrast, a $K_s$ value of 1.12 erg/cm$^2$ was obtained for the Mo/CoFeB/MgO structure. This number is similar to that of Ta/CoFeB/MgO obtained after annealing at 300 °C,[11] for which the TMR and PMA drop to nearly zero after annealing at 400 °C, further demonstrating the superior thermal stability of the Mo/CoFeB/MgO structure. More importantly, our value is smaller than the value of 2 erg/cm$^2$ obtained in Ref. 20, indicating that there is still substantial opportunity for us to improve the PMA and TMR in our MTJs.

The greatly improved PMA and TMR during high-temperature annealing are related to the unique properties of Mo compared to those of Ta. The formation energy of Fe-Ta varies from −19 to −25 kJ/mol, which is substantially lower than that of Fe-Mo in the range of −4 to 3 kJ/mol.[28] When placed next to a Fe-rich CoFeB FM layer, Mo is less likely to form alloys with Fe during annealing that could lead to the deterioration of PMA. The dead-layer thickness for each sample is calculated with a linear fit from the CoFeB thickness dependence of the areal magnetization (not shown), and the corresponding values for the Ta and Mo samples are 0.44 and 0.16 nm, respectively. Since the alloy layers are likely to be paramagnetic,[29] the large magnetic dead layer with Ta is in good agreement with the formation-energy difference between FeTa and FeMo alloys. As discussed previously,[20] the large negative formation energy of tantalum oxide and the crystalline nature of the Mo buffer layer might also contribute to the differences observed in the two types of samples. A detailed microstructural investigation on the exact pMTJ films showing large TMR is underway.

To conclude, we have demonstrated that pMTJs with Mo as the buffer and capping layers are much more stable during high-temperature annealing than pMTJs with Ta. Although the TMR of Ta/CoFeB/MgO junctions approached zero after annealing at 400 °C for 2 h, large TMR above 120% was maintained in Mo/CoFeB/MgO junctions over a wide range of MgO thickness. These results show that it is possible to achieve stronger PMA and larger TMR by selecting the proper HMs in the HM/CoFeB/MgO structure. As the diffusion of Ta has previously been identified as the main reason limiting the TMR in CoFeB/MgO junctions with in-plane magnetic anisotropy,[30] it is possible that the in-plane TMR could be substantially increased as well by replacing Ta with a more thermally stable HM, such as Mo. Finally, a stronger PMA enabled by proper HM layers could also play an important role in achieving an energy barrier of $60k_BT$ in sub-10 nm pMTJs.[31]

This work was supported in part by C-SPIN, one of six centers of STARnet, a Semiconductor Research Corporation program, sponsored by MARCO and DARPA; by the National Science Foundation (ECCS-1310338 and DMR-1420013); and by Inston Inc through a NSF Phase II SBIR award. M.R.R. is partially supported by NSF REU program Award No. PHY-1156753. S.N. gratefully acknowledges the support from Research Corporation for Science Advancement. Part of this work was carried out in the College of Science and Engineering Characterization Facility, University of Minnesota, which has received capital equipment funding from the NSF through the UMN MRSEC program under Award No. DMR-1420013. Part of this work was carried out in the College of Science and Engineering Minnesota Nano Center, University of Minnesota, which receives partial support from NSF through the NNIN program.

[1]J. S. Moodera, L. R. Kinder, T. M. Wong, and R. Meservey, Phys. Rev. Lett. **74**, 3273 (1995).
[2]T. Miyazaki and N. Tezuka, J. Magn. Magn. Mater. **139**, L231 (1995).
[3]S. S. P. Parkin, C. Kaiser, A. Panchula, P. M. Rice, B. Hughes, M. Samant, and S. H. Yang, Nat. Mater. **3**, 862 (2004).
[4]S. Yuasa, T. Nagahama, A. Fukushima, Y. Suzuki, and K. Ando, Nat. Mater. **3**, 868 (2004).
[5]W. H. Butler, X.-G. Zhang, T. C. Schulthess, and J. M. MacLaren, Phys. Rev. B **63**, 54416 (2001).
[6]J. Mathon and A. Umerski, Phys. Rev. B **63**, 220403 (2001).
[7]N. Nishimura, T. Hirai, A. Koganei, T. Ikeda, K. Okano, Y. Sekiguchi, and Y. Osada, J. Appl. Phys. **91**, 5246 (2002).
[8]M. Yoshikawa, E. Kitagawa, T. Nagase, T. Daibou, M. Nagamine, K. Nishiyama, T. Kishi, and H. Yoda, Magn. IEEE Trans. Magn. **44**, 2573 (2008).
[9]K. Yakushiji, T. Saruya, H. Kubota, A. Fukushima, T. Nagahama, S. Yuasa, and K. Ando, Appl. Phys. Lett. **97**, 232508 (2010).
[10]K. Mizunuma, S. Ikeda, H. Sato, M. Yamanouchi, H. D. Gan, K. Miura, H. Yamamoto, J. Hayakawa, F. Matsukura, and H. Ohno, J. Appl. Phys. **109**, 07C711 (2011).
[11]S. Ikeda, K. Miura, H. Yamamoto, K. Mizunuma, H. D. Gan, M. Endo, S. Kanai, J. Hayakawa, F. Matsukura, and H. Ohno, Nat. Mater. **9**, 721 (2010).
[12]W.-G. Wang, M. Li, S. Hageman, and C. L. Chien, Nat. Mater. **11**, 64 (2012).
[13]L. Thomas, G. Jan, J. Zhu, H. Liu, Y.-J. Lee, S. Le, R.-Y. Tong, K. Pi, Y.-J. Wang, D. Shen, R. He, J. Haq, J. Teng, V. Lam, K. Huang, T. Zhong, T. Torng, and P.-K. Wang, J. Appl. Phys. **115**, 172615 (2014).
[14]M. Gottwald, J. J. Kan, K. Lee, X. Zhu, C. Park, and S. H. Kang, Appl. Phys. Lett. **106**, 032413 (2015).
[15]a. Manchon, C. Ducruet, L. Lombard, S. Auffret, B. Rodmacq, B. Dieny, S. Pizzini, J. Vogel, V. Uhlíř, M. Hochstrasser, and G. Panaccione, J. Appl. Phys. **104**, 043914 (2008).
[16]I. M. Miron, K. Garello, G. Gaudin, P.-J. Zermatten, M. V. Costache, S. Auffret, S. Bandiera, B. Rodmacq, A. Schuhl, and P. Gambardella, Nature **476**, 189 (2011).
[17]C. Bi, Y. Liu, T. Newhouse-Illige, M. Xu, M. Rosales, J. W. Freeland, O. Mryasov, S. Zhang, S. G. E. te Velthuis, and W. G. Wang, Phys. Rev. Lett. **113**, 267202 (2014).
[18]U. Bauer, L. Yao, A. Tan, P. Agrawal, S. Emori, H. L. Tuller, S. van Dijken, and G. S. D. Beach, Nat. Mater. **14**, 174 (2015).
[19]D. C. Worledge, G. Hu, D. W. Abraham, J. Z. Sun, P. L. Trouilloud, J. Nowak, S. Brown, M. C. Gaidis, E. J. O'Sullivan, and R. P. Robertazzi, Appl. Phys. Lett. **98**, 022501 (2011).
[20]T. Liu, Y. Zhang, J. W. Cai, and H. Y. Pan, Sci. Rep. **4**, 5895 (2014).
[21]W.-G. Wang, S. Hageman, M. Li, S. Huang, X. Kou, X. Fan, J. Q. Xiao, and C. L. Chien, Appl. Phys. Lett. **99**, 102502 (2011).
[22]H. D. Gan, H. Sato, M. Yamanouchi, S. Ikeda, K. Miura, R. Koizumi, F. Matsukura, and H. Ohno, Appl. Phys. Lett. **99**, 252507 (2011).
[23]J. Sinha, M. Hayashi, A. J. Kellock, S. Fukami, M. Yamanouchi, H. Sato, S. Ikeda, S. Mitani, S. Yang, S. S. P. Parkin, and H. Ohno, Appl. Phys. Lett. **102**, 242405 (2013).
[24]T. Liu, J. W. Cai, and L. Sun, AIP Adv. **2**, 032151 (2012).
[25]T. Miyajima, T. Ibusuki, S. Umehara, M. Sato, S. Eguchi, M. Tsukada, and Y. Kataoka, Appl. Phys. Lett. **94**, 122501 (2009).
[26]W. G. Wang, C. Ni, G. X. Miao, C. Weiland, L. R. Shah, X. Fan, P. Parson, J. Jordan-sweet, X. M. Kou, Y. P. Zhang, R. Stearrett, E. R. Nowak, R. Opila, J. S. Moodera, and J. Q. Xiao, Phys. Rev. B **81**, 144406 (2010).

[27]S. Yuasa and D. D. Djayaprawira, J. Phys. D: Appl. Phys. **40**, R337 (2007).
[28]F. R. d. Boer, *Cohesion in Metals* (North-Holland, Amsterdam, 1988), pp. 412–548.
[29]M. Gottwald, J. J. Kan, K. Lee, S. H. Kang, and E. E. Fullerton, APL Mater. **1**, 022102 (2013).
[30]S. Ikeda, J. Hayakawa, Y. Ashizawa, Y. M. Lee, K. Miura, H. Hasegawa, M. Tsunoda, F. Matsukura, and H. Ohno, Appl. Phys. Lett. **93**, 082508 (2008).
[31]H. Sato, E. C. I. Enobio, M. Yamanouchi, S. Ikeda, S. Fukami, S. Kanai, F. Matsukura, and H. Ohno, Appl. Phys. Lett. **105**, 062403 (2014).